An Asperity Contact Model for the Slider Air Bearing

Weidong Huang and David B. Bogy
Computer Mechanics Laboratory
Department of Mechanical Engineering
University of California
Berkeley, CA 94710

Masayuki Honchi
Hitachi, Ltd.
2880 Kozu, Odawara-shi, Kanagawa-ken
256 Japan

ABSTRACT

As sliders fly closer and closer to the disks, asperity contact is inevitable due to the roughness on the sliders and the disks. A single asperity contact problem was solved using the Molecular Gas-film Lubrication (MGL) model with the non-fly-zone (NFZ) condition, which was discovered with the Direct Simulation Monte Carlo method (DSMC). It shows that the MGL model can also provide bounded pressure and resultant force in the presence of contact. Moreover, the MGL results agree well with the DSMC results. A database for a single asperity contact force and moment was then created using the MGL model with the NFZ condition. This force and moment was superimposed to the general air bearing force calculated by the MGL model when the nominal plane of the slider and the disk are not in contact. The total additional air bearing force due to asperity contact was obtained. Its effect on the slider's flying attitude was investigated and found to change the flying height and pitch angle up to 20% and 10%, respectively.

1. Introduction

Asperity contact occurs in the head/disk interface (HDI) at decreasingly small slider flying heights. When sliders fly lower, say below 15 nm, the effect of the surface roughness effect becomes significant. The height of asperities on the disk surface ranges from a couple of nanometers to about 20 or 30 nm. Under these conditions, sliders contact the taller asperities. The introduction of controlled laser texturing in the landing zone or alternatively the use of ramp loading does not avoid the problem entirely. One way to avoid stiction is to create bumps in the landing zone of disks by using a pulsed laser on a spinning disk. When the hard drive power is turned off, the slider parks on the disk in the landing zone. The laser bumps reduce the contact area between the slider and the disk and therefore reduce the stiction force. The slider contacts a certain number of the laser bumps when it parks. To simulate the dynamics of the slider take-off or landing, the air bearing pressure must be obtained. In the ramp loading method, a dynamic load/unload (L/UL) process is used. During the L/UL process, the slider may impact the disk, which leads to zero spacing, usually at one corner. The air bearing force and the contact solid-to-solid force are expected to provide enough lift to quickly move the slider away from contacting the disk. To obtain accurate air bearing force values when the L/UL dynamics are simulated numerically, we must have a good understanding of the contact air bearing mechanism.

The widely used Fukui-Kaneko MGL model is not directly applicable in solving contact air bearing problems. When the spacing is zero, the model predicts unbounded pressure and resultant force (Ruiz and bogy, 1990, Anaya-Dufresne and Sinclair, 1997).

Huang and Bogy (1998) used the Direct Simulation Monte Carlo (DSMC) method to study the single asperity contact problem. A single asperity contact problem modeled as a flat slider flying over a perfectly smooth disk surface with a spherical asperity fixed underneath the slider in point contact with the disk surface. A new boundary condition was imposed around the contact point based on the hard sphere model of the gas molecules. This boundary condition, referred to as the *non-fly-zone (NFZ) condition*, says that the molecules can not enter a spatial region that is smaller than themselves. As expected, the DSMC method successfully obtained a bounded peak air bearing pressure and a contact air bearing force. The pressure structure around the contact point was revealed. The pressure builds up in front of the asperity and there is a small vacuum region around the contact point in the non-fly-zone. Inside this region, the pressure is zero because there is no gas in it. Behind the asperity, the pressure is sub-ambient and increases with increasing distance. This pressure structure produces a small air bearing force increase, and an additional pitch moment which tends to lower the slider pitch angle.

In most cases, the slider is in contact with multiple asperities simultaneously. Having obtained the air bearing pressure distribution near a point-contact region, we now have the ability to build a model of the air bearing problem with multiple contact asperities on a disk surface. Several previous approaches to the contact asperity problem have concentrated on the solid-to-solid contact force. Cha and Bogy (1995) simulated sliders contacting multiple asperities by using a Hertz contact model. In their study, the air bearing problem was first solved assuming both the slider and disk surfaces were perfectly smooth. The contact force together with the air bearing force creates the loading

capacity. They ignored the contact effect on the air bearing force. Greenwood and Williamson (1966) created a contact model based on probability theory. The contact at the spherical asperities was assumed to be elastic and it employed the Hertzian contact model. Chang et al. (1987) followed Greenwood-Williamson's approach and added the possibility of plastic deformation to their so-called *elastic-plastic model*. Leo et al. (1995) used a model similar to the Greenwood-Williamson (GW) contact model, with a Gaussian distribution of asperity heights. They simulated the slider landing process using this model. Hu (1996) added the GW contact model and the elastic-plastic contact model into the CML Air Bearing Dynamics Simulator (which is based on the MGL model) to simulate multiple asperity contact problems. In that study, the air bearing was still obtained from two perfectly smooth surfaces and the contact effect on the air bearing was not considered since the air bearing contact mechanism was not clearly understood in the MGL model. Wahl et al. (1997) employed a contact model in the form of a power law by curve fitting experimental data (Lacey and Talke, 1992, see also Oden and Martins, 1985). Their model also disregarded the contact effects in the air bearing pressure by reasoning that this effect should be small due to the small contact area. This has been shown to not necessarily be true by the DSMC calculations, because there is a large pressure buildup in front of each contact asperity and a sub-ambient pressure region behind the asperity. Therefore the contact air bearing effect may not be negligible. On the other hand, the high pressure depends on the contact area, and the effect is small for a contact radius from 0 nm to 200 nm (see Appendix).

The contact effect on the air bearing has also been studied in other ways by numerous authors. Basically, there have been two approaches: the average film thickness

model (Mitsuya et al. 1984, 1989, and 1990) and the average flow model (Patir and Cheng, 1978 and 1979). The average film thickness model uses deterministic equations to describe the surface topography and requires extensive computer resources. In the average flow model, the roughness effects are represented by roughness-dependent coefficients, referred to as *flow factors*, which are used to multiply the mass flow rates to obtain the final mass flow rate. Following Patir and Cheng's work, there is a series of work on the flow factor method (Tripp, 1983, Hu and Zheng, 1989 and Crone et al., 1992, etc.). The main shortcoming of these two methods is the lack of solid physical foundation or interpretation.

In this report, a new model, based on the DSMC calculation together with the GW model, is proposed for incorporating the contact effect into the air bearing calculation. The model has a clear physical underpinning. It also uses the probability approach to identify the asperity contacts and to obtain the needed contact area. Since the elastic-plastic model uses a similar approach as the GW model, the newly developed contact air bearing model can also be used with the elastic-plastic model. In this report, only the GW model is considered.

2. Comparison between the Modified MGL Model and the DSMC Model

The air bearing problem could not be solved by the DSMC method if the non-fly-zone condition were not invoked. This suggests that the reason why the previous MGL model fails to predict a finite pressure distribution is that the conventional Reynolds

model is short one boundary condition (or a constraint) at the contact region, such as the non-fly-zone condition. M. Honchi (private communication) used this non-fly-zone condition in a finite element air bearing simulation program based on the MGL model. He simulated exactly the same problem discussed in Huang and Bogy (1998). The pressure at the grid points inside the non-fly-zone were set to zero while the pressure at the grid points outside the non-fly-zone were calculated as usual by the MGL model. In this way, he also obtained a pressure profile with a bounded peak pressure, and therefore, a bounded air bearing force.

Table 1 lists the contact asperity air bearing results from both the DSMC model and Honchi's MGL model with the non-fly-zone condition. The contact peak pressure and the integrated pressure are given as a function of the disk speed. The integration is over a circular area with radius twice that of the asperity base radius. The relative differences between the two models are also included in the table.

It can be seen that the largest difference for the peak pressure is just 8.8% at a speed of 25 m/s. Furthermore, for the contact air bearing force, the relative difference is within -2%. The data in Table 1 are plotted in Figs. 1 and 2. The results from the two methods appear to converge when calculating the air bearing pressure and force of a single spherical asperity contacting the disk surface. This is a very important result for modeling multiple asperity contact, since the DSMC method is a much more expensive method than the MGL model, and is impractical for use as a design tool. The above comparison suggests that the multiple contact asperity problem may be solved by using only the MGL model with some necessary modifications.

3. *Air Bearing Model for Multiple Asperity Contacts*

3.1 **Probability Contact Model** Before we develop the new model, we must first briefly explain the GW model. In 1966, Greenwood and Williamson created a contact model based on probability theory. They represented the rough surfaces as a collection of asperities with assumptions including: (i) the surface roughness is isotropic; (ii) the heights of the asperities follows a Gaussian distribution (or some other distribution functions); (iii) the asperities are spherical near their summits; (iv) all asperity summits have the same radius of curvature; (v) the asperities are far enough apart that there is no interaction between them; (vi) there is no bulk deformation, only the asperities deform elastically during contact. Hertz contact theory was used for the individual contacts in the GW model.

In the CML air bearing simulation programs, the GW model has been applied. At each grid point, there is a corresponding spacing *h*. The asperity height can be drawn from the Gaussian distribution according to *h*. The contact area and contact force can then be calculated by using Hertz equations (see Greenwood and Williamson, 1966, and Timoshenko and Goodier, 1951, for more details). The final contact force is the summation of the results at all grid points.

3.2 **New Contact Air Bearing Model Based on the GW Model** Here a few facts need to be mentioned about the GW model. First, a grid point with any spacing *h* has a probability of being in contact with the disk, no matter how smooth the disk is (except in the case of zero roughness), or how large the *h* is. In other words, each grid point

corresponds to a non-zero contact area even though in most cases this area is arbitrarily small. Second, the contact area associated with a grid point is not always a contact area corresponding to one contact asperity. It could be part of the total contact area of one contact asperity; it also could be the summation of the contact area of several contact asperities. Which is the case depends on how fine the computational mesh is and how dense the asperities are.

A few more features can be used from the GW model. The contact air bearing force is a function of the radius of curvature of the asperity, contact area, asperity density, etc. All of this information is given or can be calculated by the GW model. However, one more assumption needs to be made before we can incorporate the GW model into the contact air bearing model. In the GW model, it is assumed that asperities are isolated and independent of each other. The additional assumption in the new model is that the locations of the asperities are uniformly distributed on the disk surface.

It has been shown in Sec. 2 that the FEM results match the DSMC results reasonably well. However, for the FEM to represent the pressure profile around the contact point, the mesh must be very fine. The mesh size used by Honchi in his FEM calculation was about 2 nm. Thus, it is impractical to simulate thousands of or even tens of thousands of contact asperities directly by using the MGL model with the non-fly-zone condition. To overcome this obstacle, a so-called *table-lookup* method is used instead. The general air bearing pressure is still obtained by simulating two nominally flat surfaces. The contact effect can be superimposed on the general air bearing pressure distribution by treating asperities one by one and summing them together. The contact air bearing forces and moments for each asperity can be looked up in a ready-to-use table.

The table lists the contact air bearing forces and moments as a function of the radius of curvature of the asperity, the local linear velocity of the disk and the contact radius. In this way, the user is not likely to be aware of the additional computing time taken to calculate the total contact effect of the air bearing.

3.3 **Steady State modeling of the Multiple Asperity Contacts** When one asperity passes through the HDI, there is no doubt that it is a time-dependent process. In a typical case, there may be about 125,000 asperities under a pico slider at any given time (calculation based on data obtained by Bhushan et al., 1995), or about 400 asperities in the length direction of a pico slider (with length 1.25 mm). Suppose the disk's linear velocity is 10 m/s. Then the entire asperity array in the length direction will bring the slider a vertical motion at a frequency of at least 3 MHz, which is quite high relative to the major resonance frequencies in the HDI system. So the dynamic effect due to the passing of asperities can be ignored, and the problem can be treated as a steady state problem. The contact effect is an averaged effect over time.

3.4 **Contact Air Bearing Force Database** The table of the contact effect on the air bearing force can be generated by subtracting the air bearing force without asperities from the air bearing force with a point-contact asperity. Both cases can be calculated from the MGL model, of course with the non-fly-zone condition for the contact case. Their validity has already been discussed in Huang et al. (1997) and in Sec. 2 in this paper.

All simulations of the single contact asperity were run using Honchi's FEM program with the MGL model and the non-fly-zone condition. Two radii of curvature were selected, 2 μm and 20 μm. Nine different contact radii were used ranging from 0 nm to 200 nm. Cases with three different disk linear velocities were considered, 10 m/s, 25 m/s and 50 m/s. Since 0 m/s is a known trivial solution, it was also used to do interpolation.

The geometry for the case with 2 μm curvature is the same as described in Huang and Bogy (1998). The geometry for the case with 20 μm curvature is different. The slider dimension is 16 μm x 12.8 μm in length and width. The base diameter of the spherical bump is 1,000 nm.

The area to use for obtaining the contact effect was chosen to be twice the bump base radius. From Fig. 3 it can be seen that most of the difference in the pressure is within the chosen radius. It is roughly true for other cases as well. The pressure distribution in the effective area was transformed to a single statically equivalent force and moment. Inside the non-fly-zone, the net effect of the force is suction. The larger the contact area, the larger is the suction force. In some cases, this suction force is dominant and therefore it leads to a negative net contact air bearing force.

4. *Simulation Setup*

The Tri-Pad slider is designed to fly with a relatively large pitch in order to decrease the head/disk separation only at the rear pad. It has been observed that even at high disk speed, continuous asperity contacts can sometimes occur between the slider and

the disk, especially during the break in period before the surfaces are burnished (Machcha et al., 1996), so the Tri-Pad slider is a good candidate to use.

Two Tri-Pad slider designs are used. One is the 50% nano slider whose dimensions are 2 mm x 1.6 mm in length and width. Its suspension force is 3.5 gram. The other one is a 30% pico slider whose dimension is 1.25 mm x 1 mm with the suspension force of 2.5 gram. The rail designs of the two sliders are shown in Figs. 4 and 5. A 3.5-inch disk is selected with its roughness characterized by the asperity number density, radius of curvature of the asperity summits, and standard deviation of the asperity heights. The reduced Young's modulus for the contact was chosen to be 120 GPa. The characteristic parameters of the asperities are similar to those given in Bhushan et al. (1995). The asperity number density is 10^{11} m^{-2}. The range of the standard deviation is from 3 nm to 20 nm. The radius of curvature ranges from 2 μm to 20 μm.

Cases without the contact air bearing effect were simulated by the CML Slider Air Bearing Program (Lu, 1997). All results were obtained using a grid size of 305 x 305.

5. *Simulation Results*

5.1 **Effect of RPM** The contact effect in the air bearing was first studied by changing the rotating speed of the disk. The range of the rotating speed was from 1,000 rpm to 11,000 rpm. The 50% Tri-Pad slider was located at the disk radius of 20 mm with a skew angle of -9.5 degree. Here the sign of the skew angle follows the definition in CML steady code version 4 and the IDEMA standard, i.e. positive skew occurs when the

flow direction on the slider is from the outer rail to the inner rail. The standard deviation of the asperity heights was chosen to be 8 nm and the radius of curvature is 10 μm.

Figure 6 shows (a) the contact air bearing force and its effects on the (b) flying height at the central trailing edge, and the (c) pitch angle as a function of RPM. Over the entire rpm range, the order of magnitude of the contact air bearing force is in the tens of milligrams. The contact air bearing force is a function of the number of contact asperities and the velocity. In the low and middle range of rpm (see Fig. 6(a)), this force increases mainly due to increasing velocity. The trend changes shape at the high rpm. This can be explained by examining Fig. 6(b), which is the flying height curve. As the rpm increases, the flying height first decreases due to a rapid change of the pitch angle (see Fig. 6(c)). Then the flying height continuously increases and reduces the number of contact asperities. Even though the speed is high, the reduction in the number of contact asperities overshadows the high speed effect and leads to a lower contact air bearing force. So it can be seen that the number of contact asperities and the disk linear velocity are two balancing factors affecting the contact air bearing force. This phenomenon can be seen again later in the simulation of a “Nutcracker” slider.

When the contact air bearing force is taken into consideration, the flying height increases as compared to the case without the contact air bearing force in the calculation, as shown in Fig. 6(b). Conversely, Fig. 6(c) shows that the pitch angle is reduced by the effect of the contact air bearing force. This is because the location of the center of the contact air bearing force is very close to the trailing edge. Adding this force tends to decrease the total pitch moment and therefore decreases the pitch angle. The estimated range of the relative difference is from 0.5% to 9% for the flying height, and from -0.9%

to -3.1% for the pitch angle. The lower the rpm, the smaller the relative difference due to the smaller contact air bearing force.

5.2 **Effect of the STD of the Asperity Heights** It is expected that the heights of the asperities will influence the results. Here, three values of the STD of the asperity heights are studied: 3 nm, 8 nm and 20 nm. All three cases are calculated at 7,000 rpm. The 50% Tri-Pad slider is located at a radius of 20 mm with a -9.5 degree skew angle.

Figure 7(a) shows clearly that the higher the asperities, the larger is the contact air bearing force. In Fig. 7(b), it is seen that the difference between the two cases is not very much. From the simulation results, the GW contact force is more than 1.2 grams. It dominants the contact mechanism. But the effect of pitch angle is still very clear as seen in Fig. 7(c). The air bearing effect lowers the pitch angle up to 6.4%.

5.3 **Effect of the Radial Position and Skew Angle** Even at the same rpm, the slider flies over the disk with a different skew angle and disk linear velocity, depending on its radial position. Three positions are considered here at a disk rotating speed of 7,000 rpm: (i) a 20 mm radial position with a -9.5 degree skew angle; (ii) a 30 mm radial position with a zero degree skew angle; and (iii) a 40 mm radial position with a 10 degree skew angle. The STD of the asperity heights is 8 nm with a 10 μm asperity radius of curvature.

The results are shown in Fig. 8. When the radius increases, the disk linear velocity increases. This usually increases the contact air bearing force if the flying height is fixed. But here the total air bearing force also increases and it raises the slider's flying height. A higher flying height may reduce the number of contact asperities, therefore in some cases,

it may lower the contact air bearing force. So the final slider attitude is at equilibrium where all forces, including the general air bearing force, GW contact force and contact air bearing force, are balanced. This explains why the curve in Fig. 8(a) is an increasing-decreasing curve. The maximum contact air bearing force occurs at the 30 mm radius. The difference between the solid curve and dashed-line curve in Fig. 8(b) is about 14.5% at 30 mm, which is the largest of the three positions. As one can see in Fig. 8(c), the contact air bearing force again reduces the pitch angle. The difference between the two almost parallel curves is only from 1% to 3%.

5.4 **Effect on the 30% Pico Slider** Since the slider size is smaller, the total air bearing load capacity is decreased. The contact air bearing effect may increase and alter the flying attitude in a different way. As an example, the pico Tri-Pad slider described in Sec. 4 was used to investigate this effect. All other parameters are the same as those used in Sec. 5.1.

The results are presented in Figs. 9 to 11. As before, the flying height curve in Fig. 9(b) drops, first due to the increase of the pitch angle, as shown in Fig. 9(c). Then it starts to increase thereafter as the disk rotating speed increases. The drop in the contact air bearing force at low rpm is new. It may be because at low rpm, the pitch angle is not large. The two side rails also have asperity contacts due to the design. As the pitch angle starts to increase with rpm, asperity contacts under the two side rails begin to disappear quickly while the number of asperity contacts under the rear small pad does not change much. The result is that the number of contact asperities decreases (see Fig. 10) and leads to a reduction in the contact air bearing force.

The interesting phenomenon in this case is that the contact air bearing force increases together with the flying height in the high rpm region, as seen in Fig. 9(a) and Fig. 9(b), while Fig. 11 shows that the GW contact force decreases monotonically with rpm. It is noted that if the flying height continues to increase, the number of contact asperities will asymptotically drop to zero, and therefore so will the contact air bearing force. Obviously, the flying height is not high enough in this case to cause that result. However, it still needs to be explained why the contact air bearing force increases as the flying height increases, while the GW contact force does the opposite.

The key here is the number of contact asperities, the disk speed and the contact area. When the disk rotating speed is higher than about 5,000 rpm, all the contact asperities are concentrated at the rear pad. It can be seen from Fig. 10 that the number of contact asperities is almost constant above 5,000 rpm. Figure 12 explains this. The asperities in case (a) and case (b) in Fig. 12 are identical. The disk linear velocities and the flying heights are different, i.e. $U_a < U_b$ and $h_a < h_b$. Since both asperities are in contact with the slider, even though the contact areas are different, the number of contact asperities in both cases is the same, i.e. one. The contact air bearing force is more sensitive to the disk speed than to the contact area (as shown in Appendix). So in most cases, F^{air}_a is smaller than F^{air}_b because U_a is less than U_b. On the other hand, the GW contact force is a function of the contact area A and is *not* an explicit function of the disk speed. Therefore, F^{GW}_a is larger than F^{GW}_b because A_a is larger than A_b. It has been observed in all cases in this study that the GW contact force always decreases when the disk speed increases, whereas the contact air bearing force can either increase or decrease

when the disk speed increases, depending on the number of contact asperities in each situation.

The effect of the contact air bearing force on the flying height and pitch angle can be seen by comparing the solid line curve and dashed-line curve on Fig. 9(b) and Fig. 9(c). The higher the rpm, the larger the difference. The relative differences in the flying heights are from 2.2% at 5,000 rpm to 18.0% at 10,000 rpm. For the pitch angle, the relative differences are from -2.4% at 5,000 rpm to -8.4% at 10,000 rpm.

5.5 **Effect on the 50% Nutcracker Slider** The NSIC[†] "Nutcracker" slider has a very different rail geometry from the Tri-Pad slider, and it has a negative pressure area. Its rail shape is shown in Fig. 13. The test on the Nutcracker slider is the same as that on the 50% Tri-Pad slider described in Sec. 5.1. Figures 14(b) and 14(c) show the effect of the contact air bearing force on the flying height and the pitch angle, respectively. The relative difference in flying height is about 7.2% at 7,000 rpm. Figure 14(c) shows that the contact air bearing effect on the pitch angle for the Nutcracker slider is very small, about -1%. Figure 14(a) shows the contact air bearing force curve. It is similar to Fig. 6(a) except the value is larger here, even though the flying height shown in Fig. 14(b) is generally larger than that in Fig. 6(b). This is because the Nutcracker slider has a larger contact air bearing surface.

[†] NSIC stands for National Storage Industry Consortium.

6. *Conclusion*

A new contact air bearing model has been developed based on the single contact asperity theory discovered by use of the DSMC method. The GW probability contact model is incorporated into the new model to solve for the air bearing force in the presence of multiple contact asperities. The model is applied to the simulations of a 50% and a 30% Tri-Pad slider and a 50% Nutcracker slider. The results are compared to those of the previous contact model used in the CML steady state air bearing design code. The effect of adding the contact air bearing force can be summarized as follows:

1) The contact air bearing force tends to increase the flying height at the central trailing edge of the sliders. The amount of the difference is estimated to range from 4% to 15%;

2) The contact air bearing force tends to reduce the pitch angle up to 10%;

3) The magnitude of the contact air bearing force is in the tens of milligrams, which is sometimes equally important as the solid-to-solid contact force;

4) The contact air bearing force is an increasing function of the disk linear velocity while the GW contact force is not. It is also an increasing function of the number of contact asperities. The contact area does not have much influence on this force, although it is important in calculating the GW contact force.

5) The effect of the flying height on the contact air bearing force is not monotonic. The number of contact asperities and the disk linear velocity are two balancing factors affecting the contact air bearing force.

The increase in the flying height mentioned in 1) is in fact a combined effect of both 1) and 2). The contact air bearing force brings additional force into the total force balancing the suspension force and leads to the increase of the flying height. In addition, it also decreases the pitch angle and that also adds to the increase of the flying height at the trailing edge. So both the contact air bearing force and the contact bearing moment contribute to the increase of the flying height at the trailing edge.

The above results and conclusions seem reasonable. They are fundamentally based on the DSMC calculation which has a sound physical foundation. It also requires a relatively small amount of additional CPU time to obtain the results. However, some limitations of the model must be considered: (i) There are several assumptions made to simulate the slider flying attitude when multiple asperity contacts occur. This is due to the complexity of the roughness modeling problem. (ii) The results can be greatly improved if the contact air bearing force database covers a wider range of parameters, for example, including data with more different asperity heights, with more and higher radius of curvature, with more different disk velocity, with different pitch angle, even roll angle, etc. (iii) Comparison of the experimental results is needed to confirm the validity of this new model.

Nonetheless, the model presented here is the first contact model which takes into account both the air bearing effect and the solid-to-solid contact force to simulate the contact slider air bearing problem. Adding the contact effect of the air bearing results in a significant correction to the slider's flying attitude. With future developments through experimental work in measuring the contact effect on the slider, the air bearing contact force can be extracted from the balance of the general air bearing force (obtained by

simulation of nominally smooth surfaces with the GW model disabled), contact effect of the air bearing force (unknown), solid-to-solid contact force (measured by experiment) and the suspension force (given). The resulting contact air bearing force can be compared to the simulation results using the new contact slider air bearing model. The comparison may even be used to calibrate the air bearing contact model, if necessary, to give quantitatively correct results.

7. Reference

Anaya-Dufresne, M. and Sinclair, G. B., 1997, "On the Breakdown under Contact Conditions of Reynolds Equation for Gas Lubricated Bearings," *ASME J. of Tribology*, Vol. 119, pp. 71-75.

Bhushan, B., Yang, L., Gao, G., Suri, S., Miller, R. A. and Marchon, B., 1995, "Friction and Wear Studies of Magnetic Thin-film Rigid Disks with Glass-ceramic, Glass and Aluminum-magnesium Substrates," *Wear*, Vol. 190, pp. 44-59.

Cha, E. and Bogy, D. B., 1995, "Numerical Simulations of Slider Interaction with Multiple Asperity Using Hertzian Contact Model," *ASME J. of Tribology*, Vol. 117, pp. 575-579.

Chang, W. R., Etsion, I., and Bogy, D. B., 1987, "An Elastic-Plastic Model for the Contact of Rough Surfaces," *ASME J. of Tribology*, Vol. 109, pp. 257-263.

Crone, R. M., Peck, P. R., Jhon, M. S., Karis, T. E. and Bhushan, B., 1992, "The Flow Factor Approach in Air Bearing Simulation," *Adv. Info. Storage Sys.*, Vol. 4, pp. 123-138.

Greenwood, J. A. and Williamson, J. B. P., 1966, "Contact of Nominally Flat Surface," *Proceedings Royal Society (London)*, Series A295, pp. 300-319.

Hu, Y., 1996, "Head-Disk-Suspension Dynamics," *Doctoral Dissertation*, Dept. of Mechanical Engineering, Univ. of California, at Berkeley.

Hu, Y. and Zheng, L., 1989, "Some Aspects of determining the Flow Factors," *ASME J. of Tribology*, Vol. 111, pp. 525-531.

Huang, W., Bogy, D. B., and Garcia, A. L., 1997, "Three-Dimensional Direct Simulation Monte Carlo Method for Slider Air Bearings," *Phys. Fluids*, Vol. 9, pp. 1764-1769.

Huang, W. and Bogy, D. B., 1998, "An investigation of a Slider Air Bearing with an Asperity Contact by a Three-Dimensional Direct Simulation Monte Carlo Method," *IEEE Trans. on Magnetics*, Vol. 34, No. 4, pp. 1810-1812.

Lacey, C. A. and Talke, F. E., 1992, "Measurement and Simulation of Partial Contact at the Head/Tape Interface," *ASME J. of Tribology*, Vol. 114, pp. 646-652.

Leo, H. –L., Chapman, S. R. and Crone R. M., 1995, "Slider/Disk Interaction During the Landing Process," *ASME J. of Tribology*, Vol. 117, pp. 119-123.

Lu, S., 1997, "Numerical Simulation of Slider Air Bearings," *Doctoral Dissertation*, Dept. of Mechanical Engineering, University of California at Berkeley.

Machcha, A., McMillan, T. and Talke, F. E., 1996, "The Tribology of Tri-Pad Sliders with Hydrogenated and Nitrogenated Disks," *IEEE Trans*., Vol. 32, 5.

Mitsuya, Y., 1984, "A Simulation Method for Hydrodynamic Lubrication of Surface with Two-Dimensional Isotropic or Anisotropic Roughness Using Mixed Averaged Thickness," *Bull. JSME*, Vol. 27(231), pp. 2036-2044.

Mitsuya, Y., Ohkubo T. and Ota, H., 1989, "Averaged Reynolds Equation Extended to Gas Lubrication Possessing Surface Roughness in the Slip Flow Regime: Approximate Method and Confirmation Experiments," *ASME J. of Tribology*, Vol. 111, pp. 495-503.

Mitsuya, Y. and Hayashi, T., 1990, "Numerical Study of Film Thickness Averaging in Compressible Lubricating Films Incurring Stationary Surface Roughness," *ASME J. of Tribology*, Vol. 112, pp. 230-237.

Oden, J. T. and Martins, J. A. C., 1985, "Models and Computational Methods for Dynamic Friction Phenomena," *Computer Methods in App. Mech. and Eng.*, Vol. 52, pp. 527-634

Patir, N. and Cheng, H. S., 1978, "An Average Flow Model for Determining the Effects of Three-Dimensional Roughness on Partial Hydrodynamic Lubrication," *ASME J. of Lubrication Technology*, Vol. 100, pp. 12-17.

Patir, N. and Cheng, H. S., 1979, "Application of Average Flow Model to Lubrication between Rough Sliding Surfaces," *ASME J. of Lubrication Technology*, Vol. 101, pp. 220-230.

Ruiz, O. J. and Bogy, D. B., 1990, "A Numerical Simulation of the Head-Disk Assembly in Magnetic Hard Disk Files: Part 1—Component Models," *ASME J. of Tribology*, Vol. 112, pp. 593-602.

Timoshenko, S. and Goodier, J. N., 1951, *Theory of elasticity*, McGraw-Hill, New York.

Tripp, J. H., 1983, "Surface Roughness Effects in Hydrodynamic Lubrication: The Flow Factor Method," *ASME J. of Lubrication Technology*, Vol. 105, pp. 458-465.

Wahl, M. H., Kwon, H. and Talke, F. E., 1997, "Simulation of Asperity Contacts at the Head/Disk Interface of Tri-Pad Sliders During Steady-State Flying," *STLE*, Vol. 40, No. 1, pp. 75-80.

Table 1 Comparison of DSMC and MGL Contact Results

Speed	Contact Peak Pressure P/P_0			Force in the Affected Area (mg)		
(m/s)	DSMC	MGL	Rel. Diff.	DSMC	MGL	Rel. Diff.
0	0	0	0.00%	0	0	0%
10	2.9	2.76	-4.83%	1.487	1.469	-1.21%
25	11.58	12.6	8.81%	2.13	2.096	-1.60%

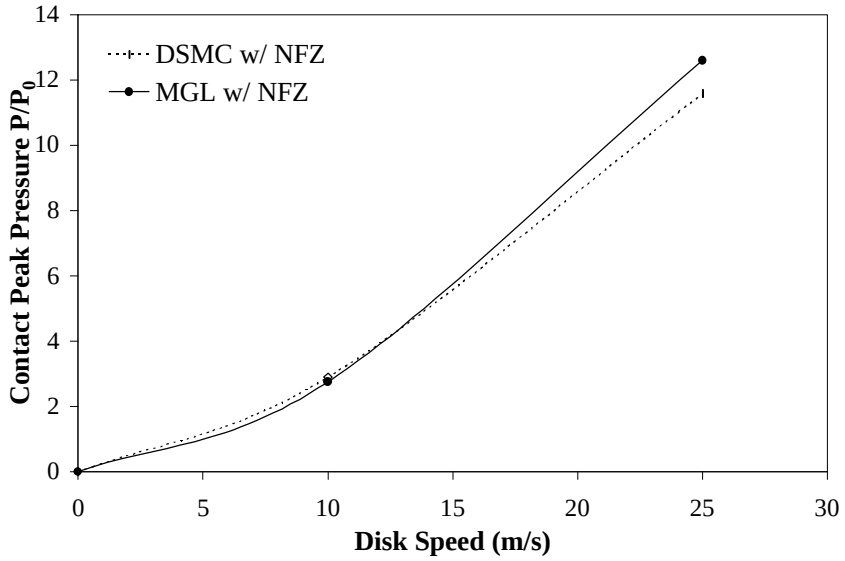

Fig. 1 Contact Peak Pressure Comparison between DSMC and MGL with Non-Fly-Zone Condition Added

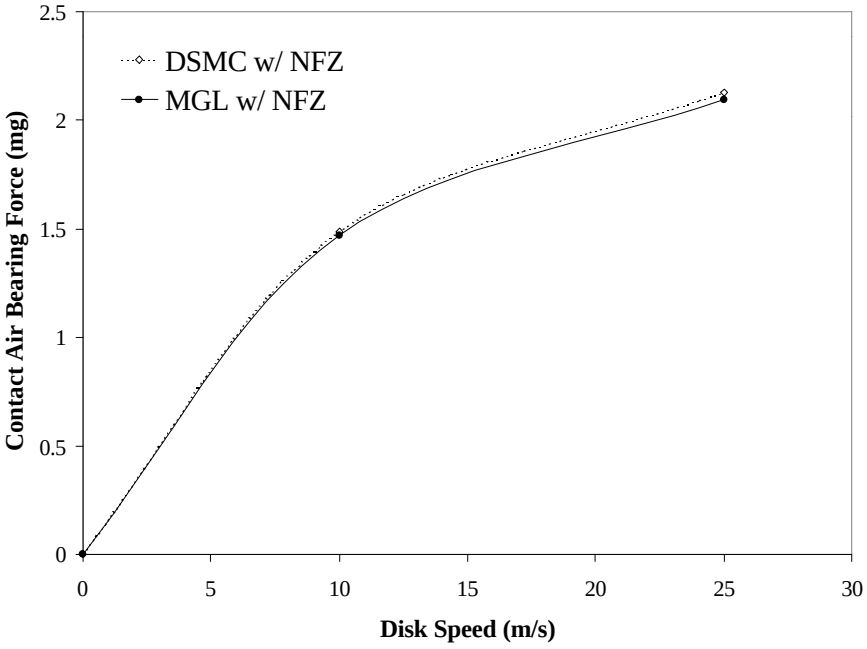

Fig. 2 Contact Air Bearing Force Comparison between DSMC and MGL with Non-Fly-Zone Condition Added

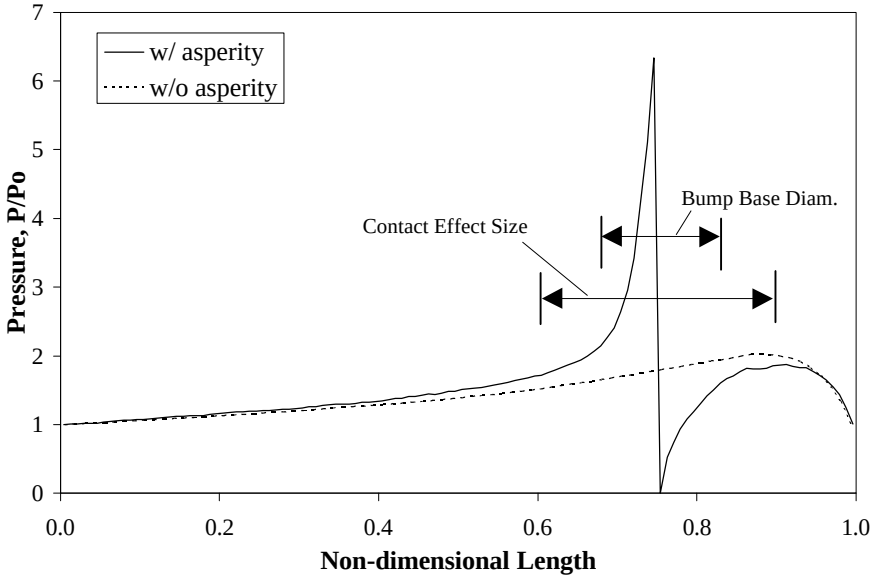

Fig. 3 Contact effect Size

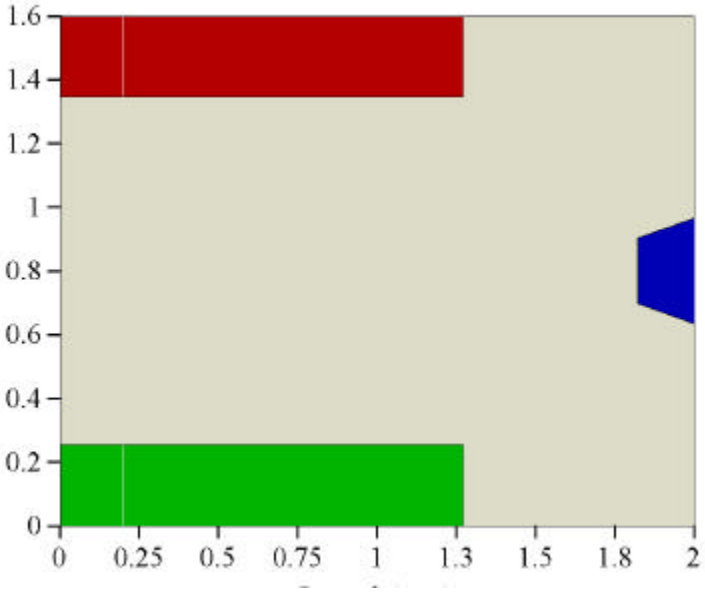

Fig. 4 Air Bearing Surface of the 50% Tri-Pad Slider

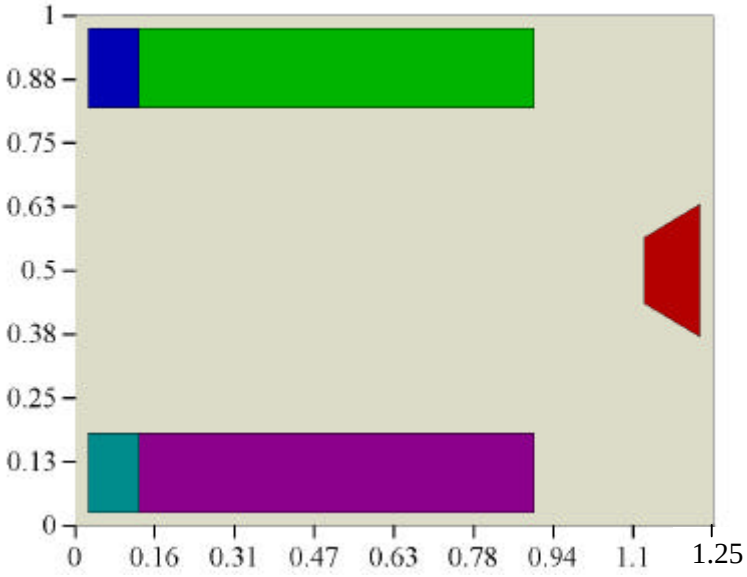

Fig. 5 Air Bearing Surface of the 30% Tri-Pad Slider

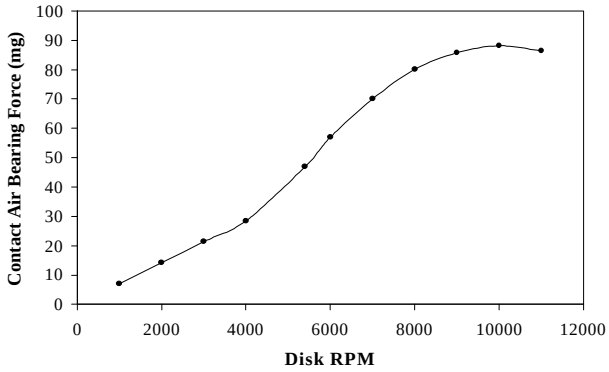

(a)

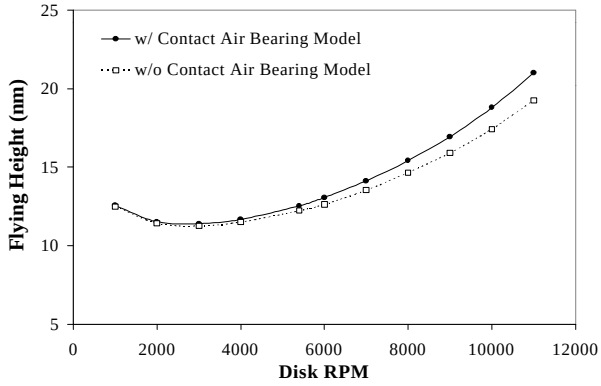

(b)

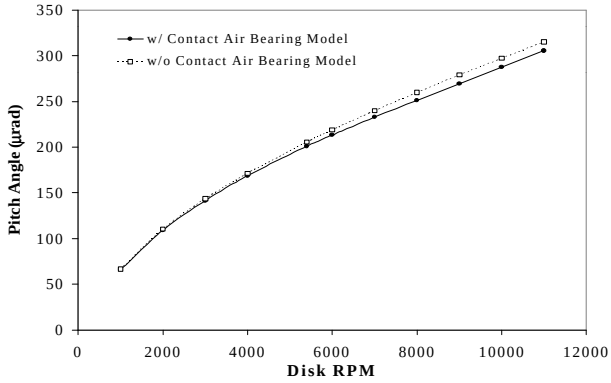

(c)

Fig. 6 Effect of RPM on the 50% Tri-Pad Slider

(a) Contact Air Bearing Force (b) Flying Height (c) Pitch Angle

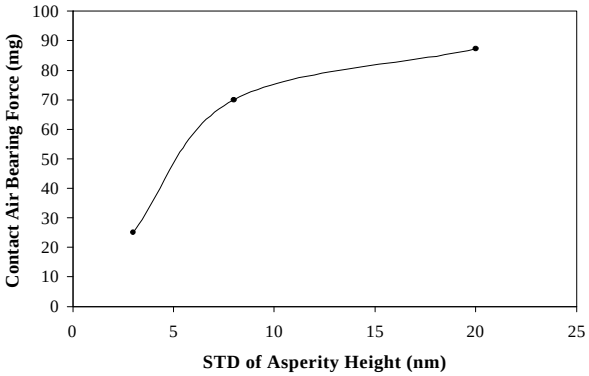

(a)

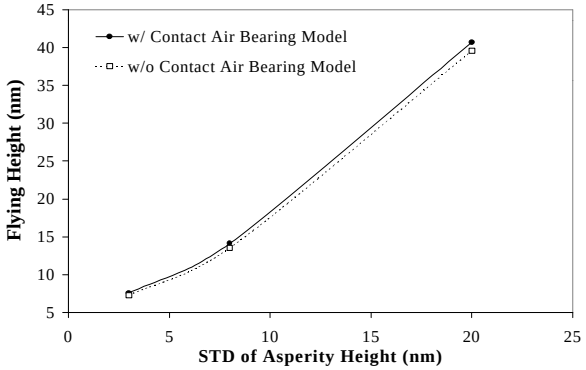

(b)

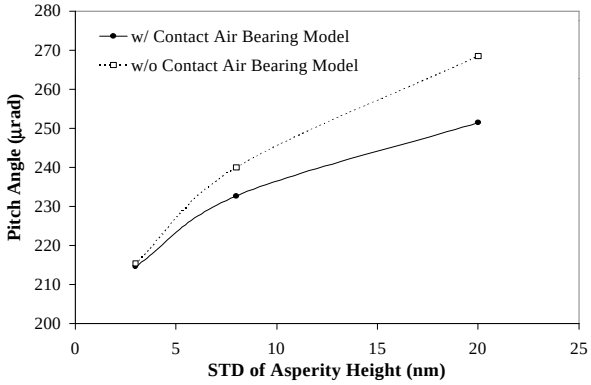

(c)

Fig. 7 Effect of the STD of the Asperity Height on the 50% Tri-Pad Slider

(a) Contact Air Bearing Force (b) Flying Height (c) Pitch Angle

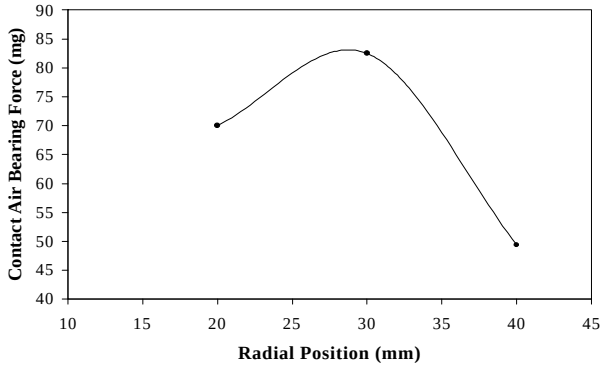

(a)

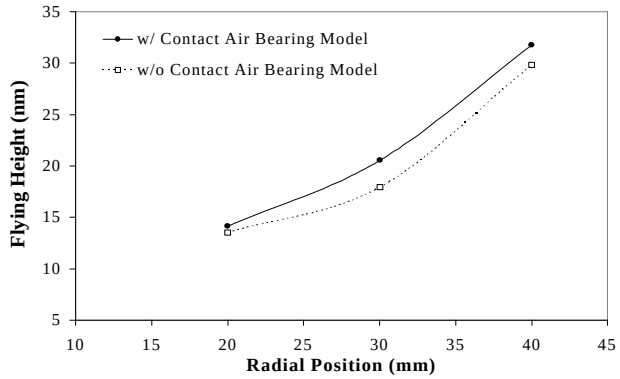

(b)

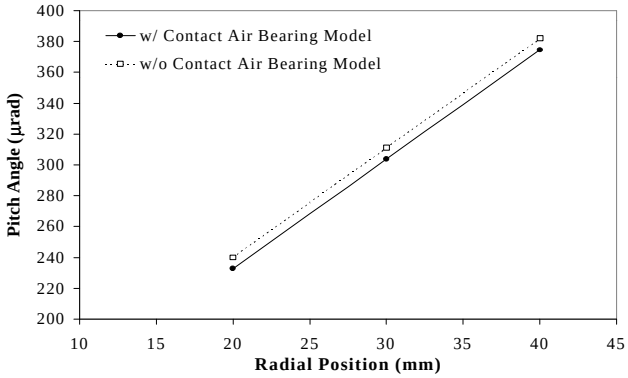

(c)

Fig. 8 Effect of the Radial Position on the 50% Tri-Pad Slider

(a) Contact Air Bearing Force (b) Flying Height (c) Pitch Angle

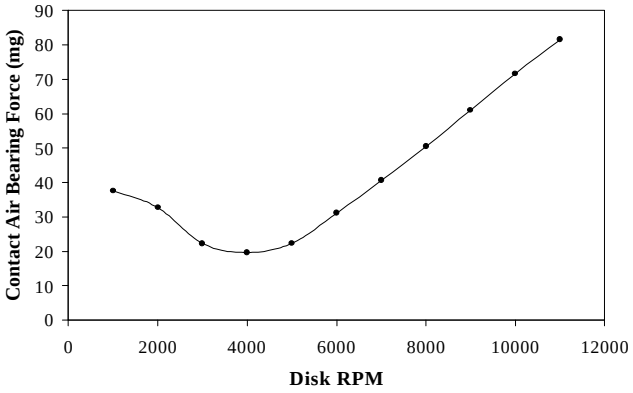

(a)

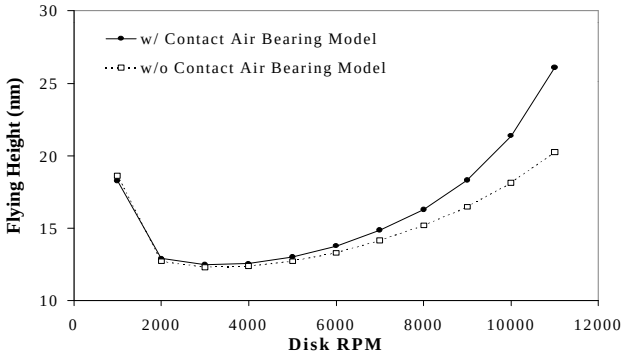

(b)

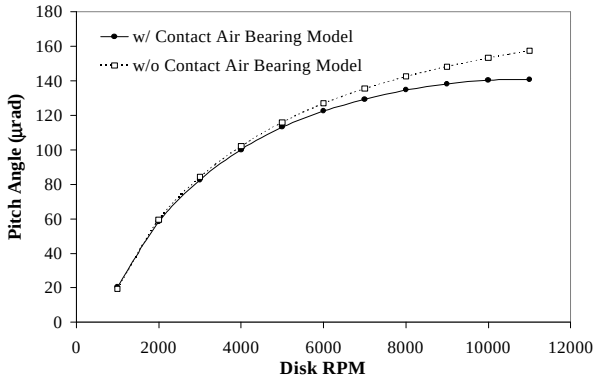

(c)

Fig. 9 Effect of RPM on the 30% Tri-Pad Slider

(a) Contact Air Bearing Force (b) Flying Height (c) Pitch Angle

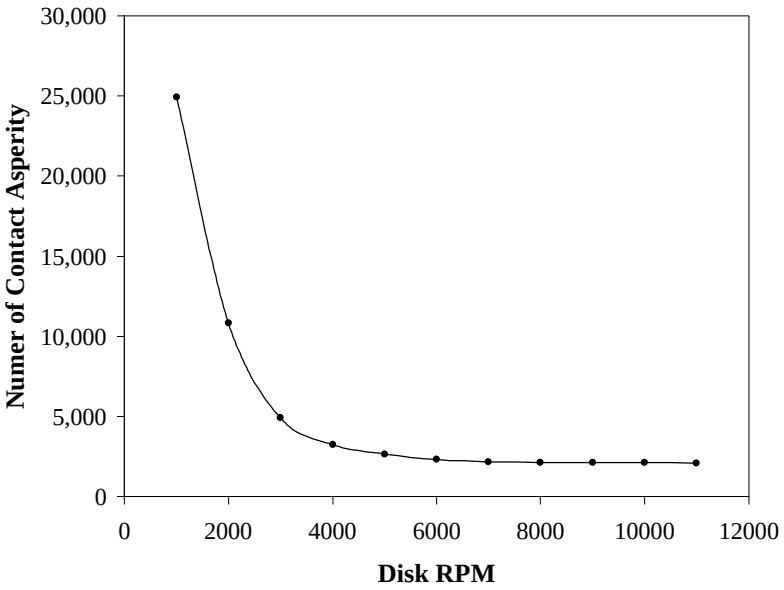

Fig. 10 Number of the Contact Asperity for the 30% Tri-Pad Slider

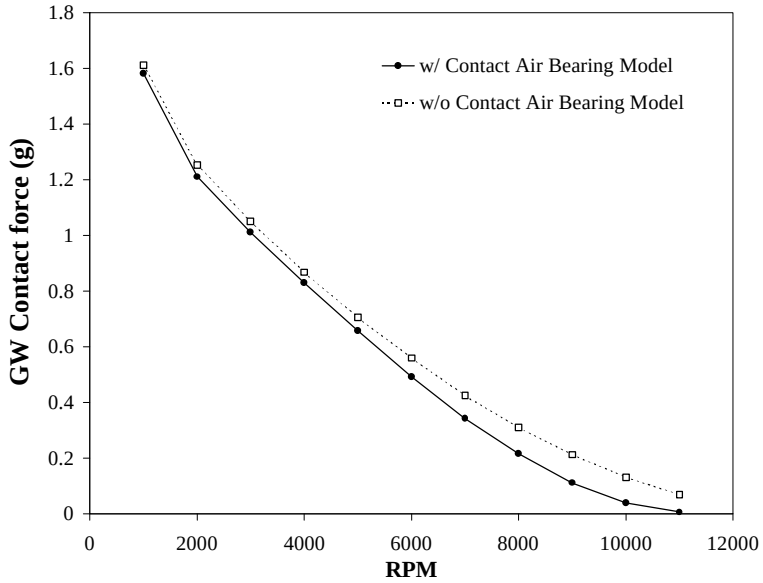

Fig. 11 GW Contact Force for the 30% Tri-Pad Slider

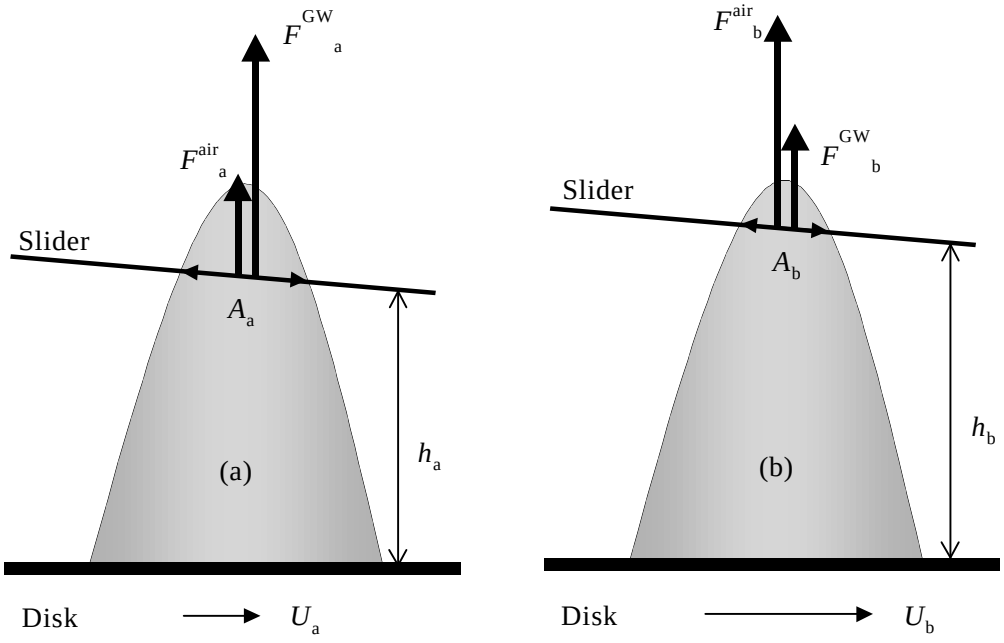

Fig. 12 Contact forces at Different Disk Speeds

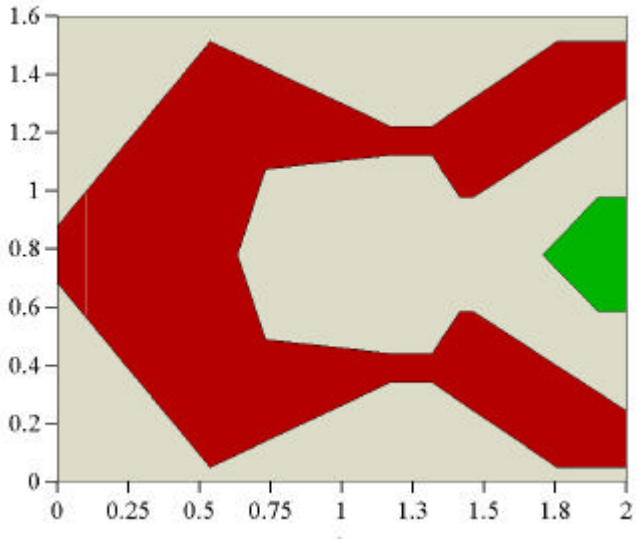

Fig. 13 Air Bearing Surface of the Nutcracker Slider

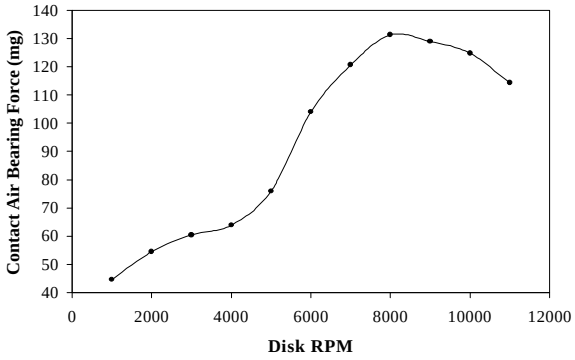

(a)

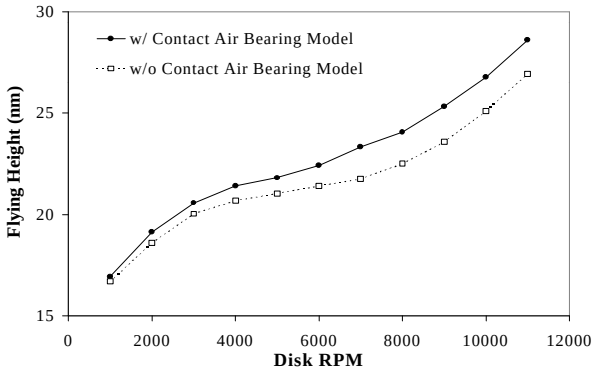

(b)

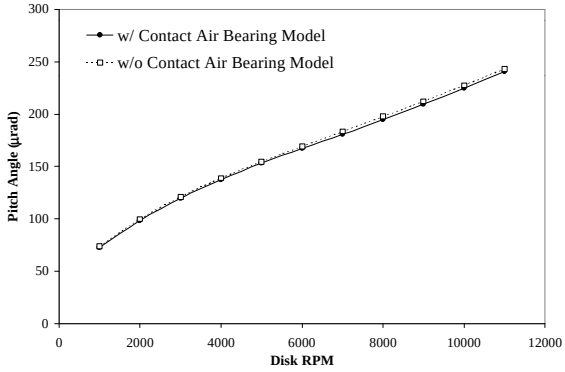

(c)

Fig. 14 Effect of RPM on the 50% Nutcracker Slider

(a) Contact Air Bearing Force (b) Flying Height (c) Pitch Angle

APPENDIX

Table (a) Contact Air Bearing Force Data

(Asperity Radius of Curvature = 2.26 μm)

Contact Radius (nm)	**Contact Air Bearing Force (mg)**			
	***U* = 0**	***U* = 10 m/s**	***U* = 25 m/s**	***U* = 50 m/s**
0	0	-4.82E-06	6.71E-05	3.04E-04
15	0	-5.39E-06	6.65E-05	3.05E-04
35	0	-7.80E-06	6.46E-05	3.13E-04
50	0	-1.09E-05	6.29E-05	3.33E-04
70	0	-2.16E-05	5.09E-05	3.37E-04
90	0	-5.20E-05	1.62E-05	3.16E-04
120	0	-5.20E-05	1.62E-05	3.16E-04
150	0	-7.32E-05	-7.13E-06	3.01E-04
200	0	-1.19E-04	-6.12E-05	2.59E-04

Table (b) Contact Air Bearing Moment Data

(Asperity Radius of Curvature = 2.26 μm)

Contact Radius (nm)	**Contact Air Bearing Moment (μN-m)**			
	***U* = 0**	***U* = 10 m/s**	***U* = 25 m/s**	***U* = 50 m/s**
0	0	2.41E-09	6.91E-09	1.18E-08
15	0	2.43E-09	6.97E-09	1.20E-08
35	0	2.49E-09	7.19E-09	1.25E-08
50	0	2.58E-09	7.49E-09	1.34E-08
70	0	2.77E-09	8.05E-09	1.48E-08
90	0	3.38E-09	9.87E-09	1.93E-08
120	0	3.38E-09	9.87E-09	1.93E-08
150	0	3.66E-09	1.10E-08	2.21E-08
200	0	4.40E-09	1.33E-08	2.77E-08

Table (c) Contact Air Bearing Force Data

(Asperity Radius of Curvature = 20.01 μm)

Contact Radius (nm)	**Contact Air Bearing Force (mg)**			
	***U* = 0**	***U* = 10 m/s**	***U* = 25 m/s**	***U* = 50 m/s**
0	0	1.66E-02	9.92E-02	2.03E-01
15	0	1.67E-02	9.93E-02	2.03E-01
35	0	1.69E-02	1.00E-01	2.05E-01
50	0	1.71E-02	1.01E-01	2.08E-01
70	0	1.76E-02	1.03E-01	2.13E-01
90	0	1.82E-02	1.06E-01	2.19E-01
120	0	1.94E-02	1.10E-01	2.31E-01
150	0	2.10E-02	1.15E-01	2.45E-01
200	0	2.45E-02	1.25E-01	2.71E-01

Table (d) Contact Air Bearing Moment Data

(Asperity Radius of Curvature = 20.01 μm)

Contact Radius (nm)	Contact Air Bearing Moment (μN-m)			
	***U* = 0**	***U* = 10 m/s**	***U* = 25 m/s**	***U* = 50 m/s**
0	0	3.09E-07	5.32E-07	4.84E-07
15	0	3.09E-07	5.32E-07	4.85E-07
35	0	3.09E-07	5.35E-07	4.89E-07
50	0	3.10E-07	5.38E-07	4.95E-07
70	0	3.10E-07	5.43E-07	5.05E-07
90	0	3.11E-07	5.51E-07	5.19E-07
120	0	3.13E-07	5.66E-07	5.47E-07
150	0	3.14E-07	5.85E-07	5.83E-07
200	0	3.17E-07	6.24E-07	6.64E-07